Pergamon

Int. J. Solids Structures Vol. 35, No. 36, pp. 5115–5138, 1998

Printed in Great Britain
0020-7683/98/$ - see front matter

PII: S0020-7683(97)00246-1

LINE-SPRING FINITE ELEMENT FOR FULLY PLASTIC CRACK GROWTH—I. FORMULATION AND ONE-DIMENSIONAL RESULTS

HYUNGYIL LEE*
Department of Mechanical Engineering, Sogang University, Seoul, Korea

and

DAVID M. PARKS
Department of Mechanical Engineering, Massachusetts Institute of Technology, Cambridge, Massachusetts 02139, U.S.A.

(*Received* 26 *November* 1996; *in revised form* 3 *August* 1997)

Abstract—A line-spring finite element model is developed to resolve fully plastic, quasi-steady, through-thickness crack growth in plane strain single-edge-cracked (SEC) specimens and surface-cracked plate/shell structures. The plane strain sliding-off and cracking model of McClintock *et al.* (1995) is adopted to obtain the instantaneous crack-tip opening angle (CTOA) in terms of material parameters and the instantaneous slip-line angle and stress triaxiality at the crack-tip. The slip-line angle and crack-tip stress triaxiality are calculated approximately using the least upper bound method of Kim *et al.* (1996a). Utilizing these approaches, the generalized forces transmitted by the line-spring finite element provide the constraint-dependent CTOA. The increment of crack extension is then determined from the kinematic relation with incremental crack-tip opening displacement through CTOA. Detailed description of the model, as incorporated into the ABAQUS (1993) finite element code in the form of a user-defined element, is given in Part I. Parametric studies in plane strain SEC specimens are carried out to examine the effects of loading type, ductility and strain hardening on plane strain crack extension behavior, and the effects of elastic surroundings on structural stability. Applications of the line-spring model to problems of surface-cracked plate and pipe are presented in Part II (Lee and Parks, 1998).

1. INTRODUCTION

The line-spring model was devised by Rice and Levy (1972) to provide an effective evaluation of the stress intensity factors (K_I) in part-through surface-cracked plates and shells. The concept was extended to elastic–plastic stationary crack analyses in the incremental theory of plasticity by Rice (1972a) and Parks and co-workers (Parks, 1981; Parks and White, 1982; White *et al.*, 1983; Lee and Parks, 1995). The most attractive feature of the line-spring model to be exploited here is that it does not require any remeshing for a simulation of arbitrary crack growth in the thickness direction. A crack-growth line-spring model based on the J-integral was attempted by Miyoshi *et al.* (1986) using deformation theory of plasticity. However, a J-based fracture is limited to amounts of crack growth small in comparison to initial ligament size (Hutchinson and Paris, 1979).

The materials commonly used in reactor piping are normally very tough and ductile. Under such circumstances, the initiation of crack growth is often preceded by fully plastic yielding of the uncracked ligament section, and some amount of stable crack growth can often be tolerated before fracture instability. Such (stable) fully plastic tearing is also of interest in design of transportation structures against overloads due to earthquakes, collisions and ship groundings (McClintock *et al.*, 1995). Under small-scale yielding conditions, the stress intensity factor (alone) characterizes the onset of brittle fracture, including even small amounts of crack growth, without regard to any detailed information on microscopic fracture mechanisms. As a comparable extension of this single parameter approach to large-scale yielding, the idea of J-controlled crack growth as proposed by Hutchinson and

* Author to whom all correspondence should be addressed.

Paris (1979) may come into mind. But the deformation theory of plasticity on which the J-integral is based is an adequate model of an elastic–plastic work-hardening only when the loading is nearly proportional. Therefore, problems involving large amounts of fully-plastic stable crack growth and unloading need to be approached with more physically sound and robust models.

Ductile crack extension is a consequence of large plastic flow causing voids to grow and coalesce; it is not due to high crack-tip stresses causing direct separation of atomic bonds as in ideally brittle materials. Crack-tip opening displacement (CTOD), and crack-tip opening angle (CTOA) are generally considered as feasible crack-tip descriptors of such strain-dominated fracture process, because they can connect the local micromechanism of crack extension to geometry-dependent stress and plastic flow. In tensile loading experiments on a plane strain double-edge cracked specimen (McClintock, 1969), and on a center-cracked plate (Gibson and Druce, 1987), the CTOA was observed to evolve during fully plastic crack growth. The changing CTOA in fully plastic crack growth is believed to result from the varying crack-tip stress triaxiality and damage accumulation ahead of the growing crack. Hancock *et al.* (1993) correlated geometry-dependence of plane strain ductile crack extension with crack-tip constraint in tests of a series of cracked specimens, including edge-cracked bend bars, compact tension specimens and center-cracked panels.

By virtue of their sliding-off and cracking model for a rigid/plastic nonhardening solid, McClintock *et al.* (1995) represented the CTOA in terms of material parameters, and the crack-tip slip-line angle and stress triaxiality. With this view, CTOA is a material-dependent function of the stress and deformation imposed on a growing crack-tip region. In concert with this notion, Kim *et al.* (1996a) provided approximate closed-form expressions for the slip-line angle and triaxiality at the crack-tip of a fully plastic deeply-cracked single-edge crack (SEC) specimen as functions of far-field tension and bending loads. When the latter two approaches are suitably combined, the constraint-dependent CTOA in a fully plastic deeply-cracked SEC specimen can be obtained from the remotely applied force and bending moment. The increment of crack extension is in turn determined from the kinematic relation with incremental CTOD through CTOA. Provided that the kinematic relationship between the CTOD-increment and increments of generalized load-point displacements is given, the plane strain crack propagation can eventually be monitored from the history of generalized load-point displacements.

In this work, following the lines of the above argument, we develop an advanced line-spring model for fully plastic quasi-steady crack growth of plane strain SEC specimens, and surface cracked plate/pipe structures. First, the meso-mechanics of estimating CTOA from the recently proposed sliding-off and cracking model is addressed, and the least upper bound method for determining crack-tip slip angle and stress triaxiality is briefly reviewed. Detailed description of line-spring constitutive relations for fully plastic crack growth is given here in Part I. The model has been incorporated into the implicit ABAQUS finite element code (1993) in the form of a user-defined element. The plane strain SEC specimen has attracted attention in connection with fracture toughness testing and as a cornerstone of the line-spring model. We thus carry out parametric studies in plane strain SEC specimens to examine the effects of loading type, initial relative crack length, ductility, flow strength (relative to modulus), and strain hardening on plane strain crack extension behavior, and the effects of elastic surroundings on structural stability. Pipes with complete circumferential cracks under uniaxial tension are studied as other 2-D problems. We then discuss the nonlinearity due to contained yielding, and instability of a plane strain SEC specimen under pure tension/bending. In Part II (Lee and Parks, 1998), the model is applied to surface crack growth problems in plates and pipes, characterized by widely varying crack-front constraint.

2. CRACK GROWTH CRITERIA

2.1. *Limitations of asymptotic solutions*

For more than two decades, concerted efforts have been made to establish fracture criteria for plane strain stable crack growth. Rice and Sorensen (1978) and Drugan *et al.*

(1982), and Drugan and Chen (1989) constructed asymptotic solutions for a crack growing in an elastic/perfectly-plastic solid under Mode I plane strain loading conditions. The solutions are effective in small-scale yielding, but are not uniquely connected to loadings in large-scale yielding. Corresponding works for linear strain hardening material were presented by Amazigo and Hutchinson (1977), and Ponte Castañeda (1987). However, under many circumstances (especially, lower strength materials) the dominant regions of the above asymptotic solutions were shown to be much smaller than the fracture process zone (Gudmundson, 1989; McClintock *et al.*, 1995). For example, when a crack advances steadily in elastic/perfectly–plastic material under plane strain mode I loading, a radius of dominance r_d of the asymptotic solution is given as $r_d \approx 0.2 r_p \exp(-\varepsilon_f/\varepsilon_y)$. Here, ε_y is the tensile yield strain, ε_f fracture strain and r_p plastic zone size. For low strength steels, with a typical value of $\varepsilon_y \approx 0.002$, and even taking ε_f as low as 0.05 under the assumption of high crack-tip stress triaxiality, and with a value of r_p as large as 100 mm under the assumption of fully plastic yielding of a test specimen, it is found that $r_d \approx 1.44 \times 10^{-5}$ μm. This value is of course much smaller than the size and spacing of the void nucleation sites responsible for ductile fracture in structural metals. Consequently, these asymptotic elastic–plastic solutions for growing cracks can hardly be applied to low strength ductile alloys, even for high crack-tip stress triaxialities. Detailed discussions on the limitations and applicability of existing asymptotic elastic–plastic solutions can be found in the works of Gudmundson (1989) and McClintock *et al.* (1995). This exercise motivates us to adopt the following rigid/plastic sliding-off and cracking model into our fully plastic crack growth line-spring formulation.

2.2. *Sliding-off and cracking model*

Ductile fracture in pre-cracked specimens consists of initial, transient and steady growth. The first two stages feature crack-tip blunting and sharp strain gradients. When concern is focused on quasi-steady crack growth, the CTOA results from the interaction of near-tip stress, deformation and damage fields with the local fracture micromechanisms. In a high ductility material, such as low-to-medium strength steels, fully plastic ductile fracture by hole growth can be regarded as rigid-plastic, since the magnitude of elastic strain is negligible compared to that of the plastic strain, at both the microscopic and plastic ligament size scales. For fully plastic, plane strain, quasi-steady crack growth in rigid/plastic nonhardening material, McClintock *et al.* (1995) considered, as shown in Fig. 1, the crack growth relative to the shoulders as the result of sliding on first the upper and then the lower slip planes, followed by cracking. The (kinematic) shear strain γ_k in the advancing shear band is the slip displacement Δu_s per unit distance, where the distance can be found by projecting Δu_s and Δa onto the normal to the slip lines:

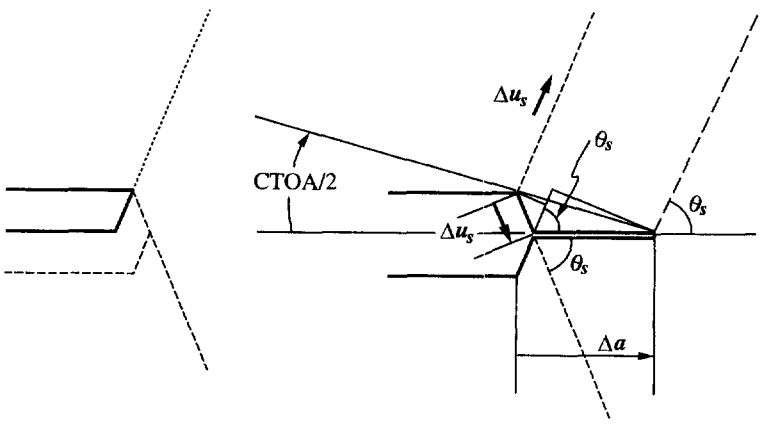

Fig. 1. Stages in sliding-off and cracking for fully plastic, plane strain, quasi-steady crack growth in rigid/plastic nonhardening material (McClintock *et al.*, 1995).

$$\gamma_k = \frac{\Delta u_s}{\Delta u_s \sin(\pi - 2\theta_s) + (\Delta a - \Delta u_s \cos\theta_s)\sin\theta_s}. \tag{1}$$

Inserting the kinematic relation $\Delta a \cdot \tan(\text{CTOA}/2) = \Delta u_s \sin\theta_s$ into eqn (1) then gives the CTOA in terms of slip angle θ_s and shear strain γ_k as

$$\tan\left(\frac{\text{CTOA}}{2}\right) = \frac{\tan\theta_s}{2/(\gamma_k \sin 2\theta_s) - 1}. \tag{2}$$

The fracture strain γ_f, which is a limiting value of the shear strain γ_k at fracture, depends on the mean normal stress at the crack-tip, σ_s, and on material properties. Accounting for hole nucleation and growth in a shear band, McClintock *et al.* (1995) suggested a semi-empirical functional form for γ_f as

$$\gamma f = \frac{(1 - 1/n)A}{\sinh[(1 - 1/n)\sigma_s/\tau_0]} + B(\sigma_s) \tag{3}$$

where τ_0 is the flow strength in shear, and n is the stain hardening exponent [plastic strain proportional to (stress)^n]. The dimensionless constant A and function B are material parameters determinable in principle from fully plastic crack growth tests. The first term on the right hand side of (3) represents a strain for hole growth to linkage by micro-rupture, and the second term represents a strain for hole nucleation. With a hole growth model in a shear band, McClintock *et al.* (1969) related the parameter A to the critical hole growth ratio at fracture such that $A = 2\ln(R_f/R_0)$, where R_0 is the initial hole size and R_f is the hole size at micro-localization between two grown holes. Note that any functional form of $\gamma_f = \hat{\gamma}_f(\sigma_s/\tau_0)$ can be used as long as it gives the essentially inverse exponential dependence of γ_f on high values of σ_s/τ_0. By equating fracture strain γ_f to the kinematically-determined strain γ_k, one can finally obtain the CTOA in terms of θ_s, σ_s and material parameters. Figure 2, obtained by McClintock *et al.* (1995) from (2)–(3), shows an inverse exponential dependence of the CTOA on $\sigma_s/(2\tau_0)$ when a nonhardening ($n = \infty$; $\tau_0 = \tau_y$) plane strain SEC specimen is subject to a flow field with $\theta_s = 45°$. Here, τ_y is the yield strength in shear. In the forthcoming line-spring model, to apply the nonhardening solutions to hardening cases in an approximate manner, we replace τ_y with an evolving "ligament-average" measure of flow strength, τ_0. On that account, "τ_0" is used instead of "τ_y" in our development, even for nonhardening cases where they coincide. Typical values of A ranging from 0.2–1.2, in an increment of 0.2, were plotted, and no nucleation strain was assumed: $B(\sigma_s) = 0$. Also shown are experimental data from singly-grooved plane strain tensile specimens of 1018 cold-finished steel with $\sigma_s/2\tau_0 = 0.5$ (Kardomateas and McClintock, 1989) and from a doubly-grooved wedge-splitting specimen of 1018 hot-rolled steel with $\sigma_s/2\tau_0 \doteq 2.2$ (McClintock and Wineman, 1987), indicating the order of magnitude difference in CTOA values obtainable under different loadings and corresponding stress triaxialities.

2.3. *Least upper bound method*

Kim *et al.* (1996a) found approximate values of the crack-tip slip-line angle, θ_s, and mean normal stress, σ_s, in terms of loads applied to a SEC specimen of rigid/plastic nonhardening material. Consider the left portion of Fig. 3, where three generalized forces are transmitted across a single circular arc spanning the ligament of a plane strain SEC specimen. For a given shear $S(=0)$ and tension N, applying the upper bound theorem to the circular arc kinematic field on the right of Fig. 3 provides an upper bound to the bending moment M. Among four kinematic variables (ϕ_1, ϕ_2, L, R) subject to two geometric constraints, ϕ_1 and ϕ_2 are selected as independent, and, the upper bound value of M can be minimized with respect to both ϕ_1 and ϕ_2. Further, assuming that the traction along the optimized arc satisfies the Hencky equation of equilibrium, and selecting a single parameter (a reference value of triaxiality on the arc) to equilibrate the prescribed shear ($S = 0$), they ultimately obtained closed form expressions for θ_s and the crack tip value of normal

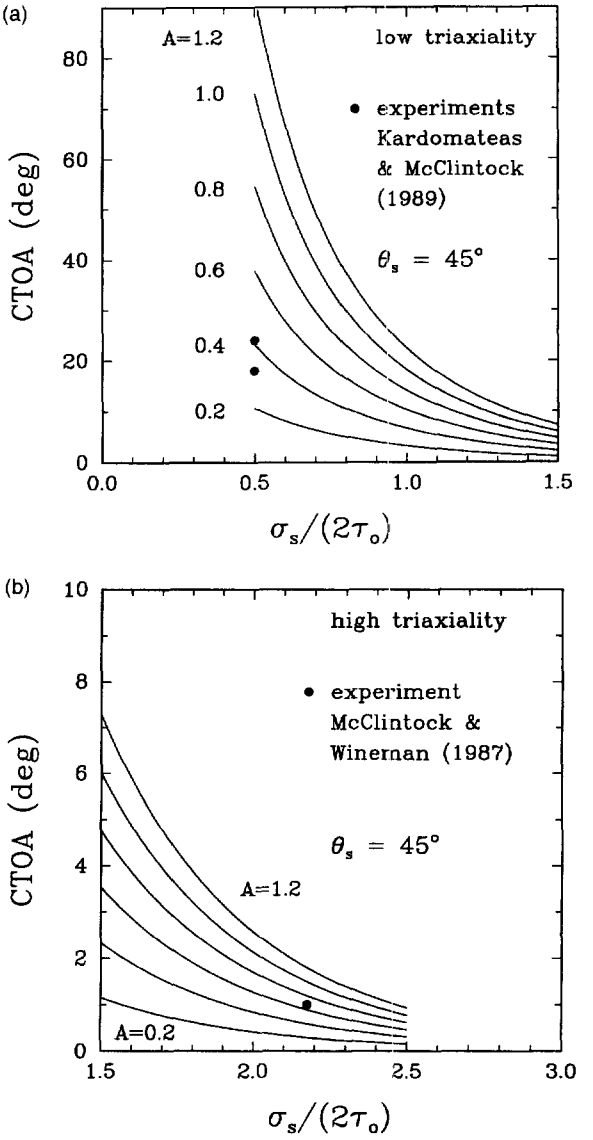

Fig. 2. CTOA vs $\sigma_s/(2\tau_0)$ for a nonhardening ($n = \infty$) plane strain SEC specimen under pure extension, $\theta_s = 45°$. Typical values of A ranging from 0.2–1.2 in an increment 0.2 were taken, and no nucleation strain was assumed: $B(\sigma_s) = 0$.

stress σ_s on the shear band, as shown by solid lines in Fig. 4(a) and (b). The parameter $\mu \equiv (M + Na/2)/(Nl)$ is introduced to measure the remotely applied bending-to-tension ratio, where $(M + Na/2)$ is the bending moment about the mid-ligament of the SEC specimen. The value of μ ranges from zero for mid-ligament tension to infinity for pure (opening) bending. The modified Green and Hundy (GH) slip-line field (1956), gives constant values of $\sigma_s = 1.54 \cdot (2\tau_0)$ and $\theta_s = 72°$ for $\mu \geqslant 0.6$.

Using a small geometry change continuum finite element model composed of an isotropic elastic/plastic material obeying nonhardening J_2 flow theory, Lee and Parks (1993) performed limit analyses of a deeply-cracked plane strain SEC specimen. In finite element limit analyses, the slip angle can be estimated from the distribution of the crack-tip shear strain $\gamma_{r\theta}(\theta)$ in polar coordinates (r, θ) centered at the crack tip. Applying suitable combinations of remote displacement and rotation large enough to bring the SEC specimen to the corresponding limit load state, they obtained values of θ_s and σ_s at various μ-values. Their nonhardening finite element results are compared with the least upper bound results in Fig. 4(a) and (b). The estimates from least upper bound method agree very well with

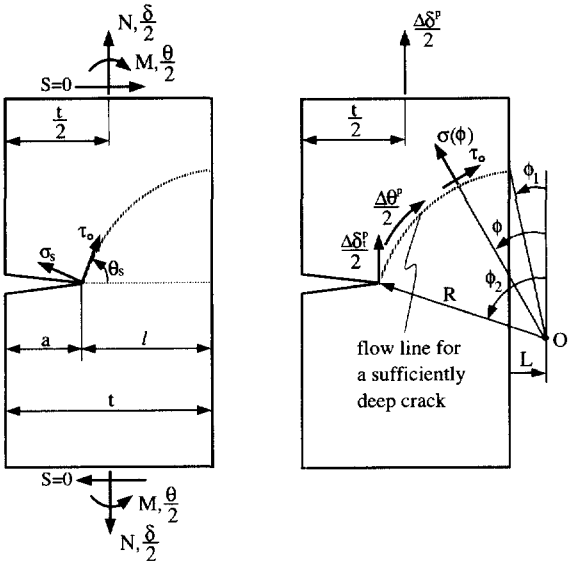

Fig. 3. Plane strain single-edge cracked specimen subject to combined tension and bending (left). Slip angle θ_s and normal stress σ_s across the flow line at the crack tip are also shown. Kinematically admissible flow field (right) used by Kim *et al.* (1996a) to generate a least upper bound yield surface, where $\Delta\delta_f^p = \Delta\delta^p + (t/2-a)\Delta\theta^p$.

finite element limit load solutions over the range of μ. Combining the least upper bound solutions with eqns (2)–(3) gives the instantaneous CTOA in the fully-plastic deeply-cracked SEC specimen as a function of μ. Figure 5 shows the predicted variation of CTOA with respect to μ in nonhardening ($n = \infty$) and low hardening ($n = 10$) plane strain SEC specimens for the values of $A = 0.2$–1.2 and $B(\sigma_s) = 0$.

3. THE LINE-SPRING MODEL

3.1. *Preliminaries*

The virtue of the line-spring model is that it brings certain complicated 3-D cracked structures within the realm of plate/shell problems, in the way described below. Consider a part-through surface crack of total length $2c$ in a shell of thickness t, as shown schematically in Fig. 6. The coordinate x measures the distance from the center line ($x = 0$) of the surface crack. The local depth of the surface crack is $a(x)$, where $0 \leqslant a(x) \leqslant t$ for $|x| \leqslant c$. The presence of a part-through surface crack in a shell structure introduces additional compliance, which is accounted for by a model through-crack of length $2c$ in the shell, the faces of which are connected by a generalized spring-foundation. The compliance of the foundation varies along the cut according to the local crack depth $a(x)$ of the surface crack. In symmetrically-loaded structures, the spring-foundation transmits a membrane force $N(x)$ and a bending moment $M(x)$ per unit length. Work-conjugate variables are relative separation and rotation $[\delta(x), \theta(x)]$ of the model through-crack. Construction of the line-spring model is completed by equating the local compliance of the foundation at x to the additional cracked compliance of a plane strain SEC specimen having the same thickness t and crack depth $a(x)$ (Rice and Levy, 1972; Rice, 1972a). Thus, the problem is reduced from 3-D to 2-D by lumping the additional compliance onto the springs distributed along the line of the cut in a shell. Finally, the crack front deformation parameter at position x (as measured by $K_I(x)$, CTOD(x), etc.) is estimated as the same value which would occur in the plane strain SEC specimen of thickness t and crack depth $a(x)$ undergoing the combined load histories $[N(x), M(x)]$.

In the linear elastic domain, the generalized forces and displacements, renamed as $Q_1 = N$, $Q_2 = M$; $q_1 = \delta$, $q_2 = \theta$, are connected by the elastic matrix P_{ij}:

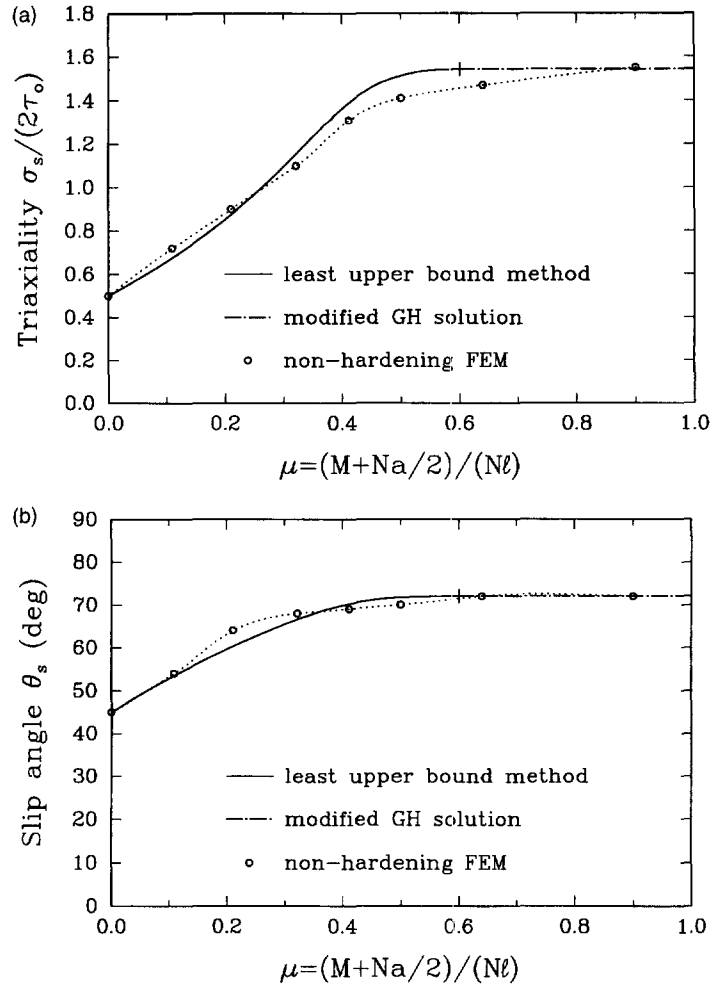

Fig. 4. (a) Normal stress σ_s across the flow line at the crack-tip of a deeply-cracked SEC specimen as a function of remotely applied net section tension-to-bending ratio, μ. (b) Slip angle θ_s at the crack-tip of a deeply-cracked SEC specimen as function of μ.

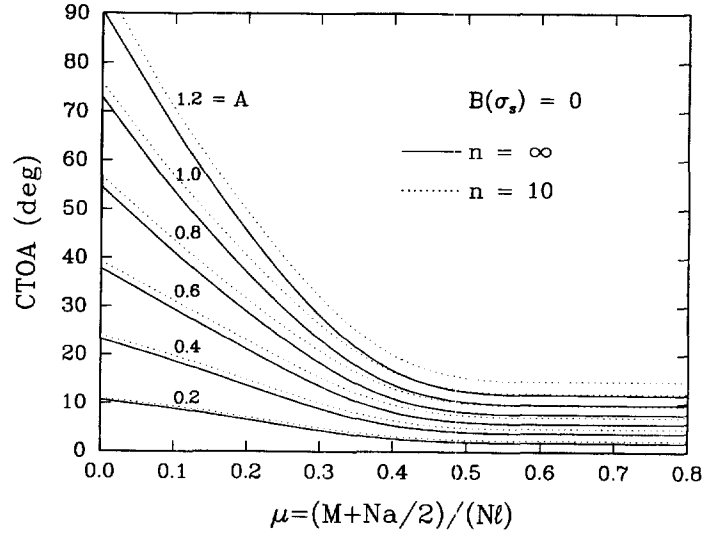

Fig. 5. Predicted CTOA variation with respect to the net section bending-to-tension ratio, μ in nonhardening ($n = \infty$) and low hardening ($n = 10$) plane strain SEC specimens for the material properties $A = 0.2$–1.2 and $B(\sigma_s) = 0$.

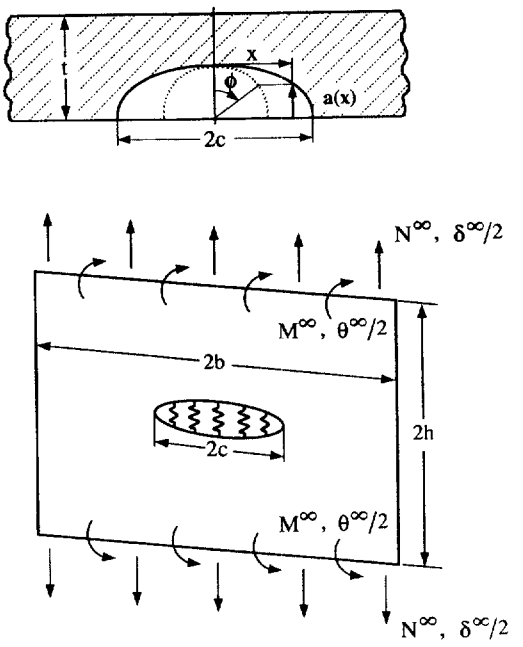

Fig. 6. Cross section of a part-through surface crack with length $2c$ and varying depth $a(x)$ in a shell of thickness t (above). Schematic illustration of line-spring model which converts the part-through surface crack to the through-crack with a generalized foundation (below).

$$q_i^{(e)} = P_{ij}(a_0, t)Q_j \tag{4}$$

where a_0 is the original crack length prior to the initiation of crack extension. The summation convention (from 1 to 2) on repeated subscripts is implied. Before the onset of "initial" fully plastic yielding, the deformation is assumed to be purely elastic, as denoted by superscript "(e)". The elastic compliance matrix P_{ij} is determined from the mode I stress intensity factor calibrations of the SEC specimen using the energy/compliance relation (Rice, 1972b)

$$P_{ij} = \frac{2}{E'}\int_0^{a_0} F_i(\bar{a}, t)F_j(\bar{a}, t)\,\mathrm{d}\bar{a} \tag{5}$$

where $E' = E/(1-\nu^2)$, E is Young's elastic modulus, and ν is Poisson's ratio. The functions $F_i(a, t)$ $(i = 1, 2)$ contain the K_I-calibrations of the SEC specimen subject to tension (F_1) and bending (F_2); that is, $K_I(a, t) = F_i(a, t)Q_i$ by superposition. These calibration functions are obtained from the handbook, for example, of Tada *et al.* (1985).

3.2. *Yield surfaces*

A convex yield function $\Phi(Q_i; a, t; \tau_0) = 0$ in the generalized force space is required for a formulation of fully plastic line-spring based on the flow theory of plasticity. Kim *et al.* (1996b) proposed an elliptical yield surface, which automatically satisfies convexity, for a deeply-cracked SEC specimen as

$$\Phi_K = \left[\frac{N/(2\tau_0 l) - 0.4953}{0.5047}\right]^2 + 9.0256\left[\frac{M + Na/2}{2\tau_0 l^2}\right]^2 - 1 = 0 \tag{6}$$

where a is the crack length and l is the remaining ligament $(t = a + l)$. The flow strength in shear τ_0 is related to the flow strength in tension σ_0 by $\tau_0 = \sigma_0/\sqrt{3}$ according to a Mises yield criterion. The constants $(-0.4953;\ 0.5047;\ 9.0256)$ were obtained by matching the

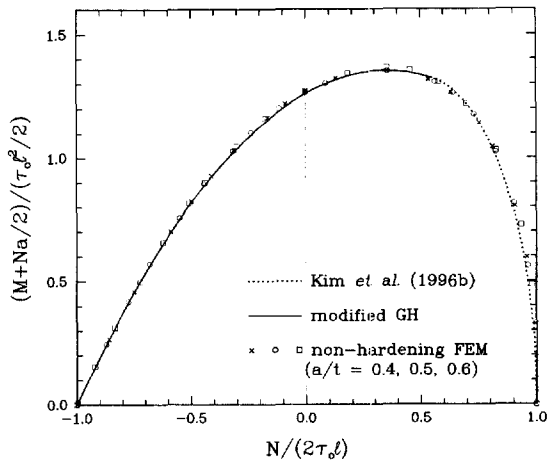

Fig. 7. Combined tension and bending yield surfaces in the generalized force space, the coordinates of which are normalized with the SEC specimen ligament, l and shear flow strength, τ_0. Circled data points are from nonhardening FEM limit analyses (Lee and Parks, 1993). Also shown are the modified Green and Hundy yield surfaces (White *et al.*, 1983) and the quadratic form by Kim *et al.* (1996b).

slopes and values of the elliptical yield locus at $N/(2\tau_0 l) = 1$ and 0.55 with those of the known slip-line field solutions at these points.

When an opening bending moment, joined by an axial force of a suitably restricted magnitude, is applied to the SEC specimen, the Green and Hundy (1956) (GH) field for pure bending can be modified to produce a slip-line field for the combined load state. Equilibrating the applied force and moment with the resultants of the modified GH slip-line fields, White *et al.* (1983) obtained the following yield surface:

$$\Phi_{\mathrm{MGH}} = \frac{M}{\tau_0 l^2} - \frac{N}{2\tau_0 l}(0.26 - a/l) + 0.37\left(\frac{N}{2\tau_0 l}\right)^2 - 0.63 = 0. \tag{7}$$

For axial forces ranging from $N = -2\tau_0 l$–$N = 0.55 \cdot (2\tau_0 l)$, the yield surface given by eqn (7) is possibly exact for deep cracks.

The above two yield surfaces apply to deep cracks, where plastic deformation is confined to the remaining ligament. As discussed by Green (1956) and Ewing (1968), the slip-line field of shallow cracks under predominant bending spreads to the front surface. Lee and Parks (1993) constructed an accurate set of tabulated yield surfaces of plane strain SEC specimens for various crack depths. From the variation of yield surface shape with respect to the relative crack depth, they suggested that deep cracks might be classified as those having relative crack depth a/t greater than about 0.35. Figure 7 shows the deep-crack yield surfaces plotted in a generalized force space, the coordinates of which are normalized with the shear flow strength τ_0 and the ligament l of the SEC specimen. The quantity $(M + Na/2)$ is the moment measured about the mid-ligament of the SEC specimen. Data from continuum finite element limit analyses (Lee and Parks, 1993) are exhibited by the cross symbol, circle and square for $a/t = 0.4$, 0.5 and 0.6, respectively. Modified GH solutions and numerically-obtained data show excellent agreement for $-1 \leqslant N/(2\tau_0 l) \leqslant 0.55$. In its intended range of applicability, namely $0.55 \leqslant N/(2\tau_0 l) \leqslant 1$, the approximate yield locus (6) is within 2% of the numerically-obtained yield surfaces. Therefore, the combination of (6) and (7) affords a complete and explicit set of yield functions for a broad range of loading applied to a deeply-cracked plane strain SEC specimen.

3.3. *Elastic–plastic crack-growth line-spring*

In the following formulation of a fully-plastic crack-growth line-spring model, we assume an isotropic hardening in which the yield surface expands due to hardening, and

contracts due to crack growth, into the adjacent concentric locus without changing shape. A work-hardened yield surface $\Phi(Q_i; a, t; \tau_0) = 0$ will be called simply the "yield surface", while the yield surface $\Phi(Q_i; a, t; \tau_y) = 0$ defined on the shear yield strength τ_y is termed by the "initial" yield surface.

The generalized forces are represented in terms of the elastic stiffness matrix and the elastic generalized displacements:

$$Q_i = S_{ij}(a, t) q_j^{(e)} \tag{8}$$

where the elastic stiffness matrix $S_{ij}(a, t) \equiv P_{ij}^{-1}(a, t)$ is evaluated based on the current crack length a. The total generalized displacement increments Δq_i are additively decomposed into an elastic and a plastic part: $\Delta q_i = \Delta q_i^{(e)} + \Delta q_i^{(p)}$. The plastic generalized displacement increments under active plastic loading are taken as the product of a nonnegative scalar, Λ, and the yield surface normal,

$$\Delta q_i^{(p)} = \Lambda \Phi_{,i} \equiv \Lambda \frac{\partial \Phi}{\partial Q_i}. \tag{9}$$

Here the nonnegative scalar Λ depends on the load increments, gross work-hardening and the amount of crack extension. The consistency condition that the force state remains on the yield surface during plastic flow gives

$$\Phi(Q_i; a, t; \tau_0) = 0. \tag{10}$$

The crack length a at the end of a time increment can be expressed as

$$a = a^{(\tau + \Delta\tau)} = a^{(\tau)} + \Delta a = a_0 + (\Delta a)^{\text{tot}} \tag{11}$$

where the superscript τ denotes the time. Here Δa represents the crack growth increment across a time-increment $\Delta\tau = (\tau + \Delta\tau) - \tau$, whereas $(\Delta a)^{\text{tot}}$ represents the total accumulation of crack increments—the difference between the current crack length a at $\tau + \Delta\tau$ and the original crack length a_0 at $\tau = 0$. In a fully-plastic 2-D plane strain crack growth model, once a crack starts to grow by satisfying certain initiation criteria (and is presumed to enter a steady stage of crack growth), Δa can be kinematically related to $\Delta\delta_t$ through the CTOA. CTOD ($= \delta_t$) is taken as the sum of two terms, "linear-elastic" and "plastic" parts: $\delta_t = \delta_t^{(e)} + \delta_t^{(p)}$. Choosing δ_t as an initiation criterion, and using the rigid-plastic kinematic relations among Δa, CTOA and $\Delta\delta_t$ (McClintock *et al.*, 1995), we may write

$$\Delta a = \begin{cases} 0 & \text{if } \delta_t < \delta_t^c \\ \Delta\delta_t^{(p)} / [2 \tan(\text{CTOA}/2)] & \text{if } \delta_t \geqslant \delta_t^c \end{cases} \tag{12}$$

where δ_t is the CTOD at the initial (stationary) crack-tip, and the material fracture property δ_t^c is the critical CTOD at initiation. Since our interest here lies in fully plastic crack growth, crack extension associated with $\Delta\delta_t^{(e)} (\ll \Delta\delta_t^{(p)})$ is neglected in (12). The position of a growing crack-tip changes continuously; thus, $\Delta\delta_t^{(p)}$ (assumed to be $\approx \Delta\delta_t$) is rather interpreted as the relative separation, at time $\tau + \Delta\tau$, of two crack flank points, which once formed the crack-tip at time τ (Rice, 1975). Note that our crack growth line-spring model assumes that the crack initiates after initial fully plastic yielding, $\Phi(Q_i; a, t; \tau_0) = 0$, as is often observed in ordinary-sized parts composed of ductile material. Further, Lee and Parks (1993) provided $\Delta\delta_t^{(p)}$ of a fully plastic SEC specimen in the form

$$\Delta\delta_i^{(p)} = \Delta\delta^{(p)}\left[1 + L_2 \cdot \left(\frac{1}{2} - \frac{a}{t}\right) \cdot \left(\frac{t\Delta\theta^{(p)}}{\Delta\delta^{(p)}}\right)\right] \tag{13}$$

where a/t is the relative crack depth, and $\Delta\delta^{(p)}/(t\Delta\theta^{(p)})$ is the ratio of load-point plastic displacement increment to plastic rotation increment multiplied by the SEC specimen thickness. L_2 is a function of (a/t) and $[\Delta\delta^{(p)}/(t\Delta\theta^{(p)})]$, representing the degree of negative relative rotation of the crack flank with respect to the far field rotation. Constitutive relations (8)–(13) are sufficient to describe fully plastic crack growth behavior of the line-spring model within a "nonhardening" idealization.

In case of hardening, the line-spring ligament-average flow strength τ_0 and the ligament-average plastic strain $\gamma_0^{(p)}$ find their connection through the plastic material hardening modulus $h_s(\gamma_0^{(p)})$, which is the slope of the stress/plastic strain curve in shear, as

$$\Delta\tau_0 = \int_{\tau_0}^{\tau_0 + \Delta\tau_0} d\tau_0 = \int_{\gamma_0^{(p)} + \Delta\gamma_0^{(p)}}^{\gamma_0^{(p)}} h_s \, d\gamma_0^{(p)}. \tag{14}$$

At the macroscopic level, the plastic work increment per unit thickness of the SEC specimen, $\Delta W^{(p)}$ is given by

$$\Delta W^{(p)} = Q_i \Delta q_i^{(p)}. \tag{15}$$

This plastic work increment can also be expressed by the integral of the continuum plastic work increment over the area $A^{(p)}$ of the SEC specimen where plastic dissipation is occurring,

$$\Delta W^{(p)} = \int_{A^{(p)}} \sigma_{ij} \Delta\varepsilon_{ij}^{(p)} \, dA^{(p)} = \int_{A^{(p)}} \bar{\tau} \Delta\bar{\gamma}^{(p)} \, dA^{(p)}. \tag{16}$$

Here the quantities $\bar{\tau}$ and $\Delta\bar{\gamma}^{(p)}$ are local values of equivalent shear stress and equivalent plastic shear strain increment in the dissipation area $A^{(p)}$. Parks (1981) inferred that the active plastic deformation area $A^{(p)}$ of the deep crack would be proportional to the square of a "characteristic length". With the ligament l chosen as the characteristic length, the last integral (16) can be evaluated approximately, in terms of τ_0 and $\Delta\gamma_0^{(p)}$, as

$$\Delta W^{(p)} = f \cdot \tau_0 \cdot \Delta\gamma_0^{(p)} \cdot l^2 \tag{17}$$

where the dimensionless scalar f, which we call the strain hardening factor, is expected to be of order unity. Assuming isotropic hardening, equivalency of macroscopic and continuum plastic work increments reduces to

$$f \cdot \tau_0 \cdot \Delta\gamma_0^{(p)} \cdot l^2 = Q_i \Delta q_i^{(p)}. \tag{18}$$

Equations (8)–(14), (18) represent a complete set of constitutive relations for fully plastic, hardening, crack growth behavior of the line-spring model. In the absence of crack growth ($\Delta a = 0$), the set of equations exactly recovers the stationary crack model. For the stationary crack in a low hardening material ($n = 10$), Lee and Parks (1995) calibrated the value of strain hardening factor as $f = 0.9$ by comparing the behavior of a single line-spring to that of the continuum finite element solution of a plane strain initial boundary value problem having the same dimensions, material properties, and loading histories. Here, we simply take $f = 0.9$ obtained from stationary crack analyses to be use in the applications of crack growth line-spring model to the nonhardening and low hardening materials.

4. RESULTS

For unconditional stability in our numerical time integration procedure, we employed the Euler Backward formulation so that the line-spring constitutive equations are satisfied at the end of a time increment. At the beginning of a time increment, estimates of Δq_i are presumed known. For given Δq_i, we (i) assume $\Delta q_i^{(p)}$, and (ii) find the corresponding ΔQ_i, Δa, $\Delta\gamma_0^{(p)}$ and $\tau_0(\gamma_0^{(p)}+\Delta\gamma_0^{(p)})$ from (8), (12) and (18) by two-level Newton–Raphson iterations. Then, (iii) $\Delta q_i^{(p)}$ and $\Delta\gamma_0^{(p)}$ are corrected [by $d(\Delta q_i^{(p)})$ and $d(\Delta\gamma_0^{(p)})$, respectively] to satisfy the normality (9) and consistency (10) conditions. Corrected values of the plastic displacement increments $[=\Delta q_i^{(p)}+\mathrm{d}(\Delta q_i^{(p)})]$ are substituted for assumed values of $\Delta q_i^{(p)}$ in (i) and the remaining steps (ii) and (iii) are repeated until the corrections $\mathrm{d}(\Delta q_i^{(p)})$ are within specified tolerances, or equivalently, until the implicit constitutive eqns (8)–(14), (18) are satisfied simultaneously. Subsequently, we find the elastic–plastic Jacobian matrix $T_{ij}^{(ep)} \equiv \partial Q_i/\partial q_j$, which is used for revising the estimates of nodal displacements Δq_i in the main body of the ABAQUS finite element program (1993).

In Part I here, simulating fully plastic crack growth in plane strain SEC specimens, we examine the effects on crack extension behavior of specimen size and relative crack depth, loading conditions, and material properties such as material ductility (A-constant of the model), flow strength (relative to modulus), strain hardening, and critical CTOD at crack initiation.

Figure 8(a) shows the normalized axial force, $N/(2\tau_y l_0)$ vs normalized loading-point total displacement, $\delta^{\mathrm{tot}}/l_0$, of the plane strain SEC specimen with initial relative crack depth $a_0/t = 0.5$ under pure extension ($N > 0$, $\theta^{\infty} = 0$; θ^{∞} is the rotation at the far-field loading-point). The axial force is normalized by the initial yield strength in shear τ_y, and initial ligament length l_0. We selected the total displacement δ^{tot} as a parameter in order to study the effect of specimen length $2L_s$ on the stability of the crack. For all continuum and line-spring finite element input data, we employed a multi-linear stress/strain curve, smoothly approximating the experimental data for ASTM A710 Grade A steel. In A710 steel, the strain hardening exponent is near $n \doteq 10$ and $\sigma_u/\sigma_y \doteq 1.35$, where σ_u is the tensile strength occurring at about 8% strain (Reuter and Lloyd, 1990). The critical CTOD value at crack initiation for this material ranges from $\delta_i^c = 0.2$ to 0.35 mm, depending on track-tip constraint (Hancock *et al.*, 1993). The initial crack depth, $a_0/t = 0.5$ is deep enough to constrain plastic deformation to the ligament for all loading conditions (Lee and Parks, 1993). The values of the material crack ductility parameters $A = 0.5$ and $B(\sigma_s) = 0$ correspond to the critical hole growth ratio $R_f/R_0 = 1.32$ and fracture strain $\gamma_f = 0.44$ under crack-tip stress triaxility $\sigma_s/(2\tau_0) = 0.5$. Since the grip condition $\theta^{\infty} = 0$ is applied to the far-field loading point, the line-spring load state (N, M) is not precisely at the vertex point of the yield surface, characterized by load state $N = 2\tau_0 l$ and $M = -Na/2$. The cross symbol indicates the incipient fully plastic yielding $\Phi(Q_i; a, t; \tau_y) = 0$, and the open circle indicates the initiation of the crack growth. Solid lines were obtained based on the critical CTOD value, $\delta_t^c/l_0 = 0.01$ and dashed lines were based on $\delta_t^c/l_0 = 0.02$. In this model, the axial force in pure extension continues to increase after crack initiation, reaching a maximum value soon afterwards. This reaction force increase comes in part from the drift of the load state towards the vertex point of the yield surface, and in part from the increase of average flow stress τ_0 due to the model strain hardening. In short and intermediate length specimens ($L_s/t = 3$, 10), the value of δ_t^c does not significantly affect the overall load–deflection response. But in the long specimen ($L_s/t = 20$), where the reaction force decreases directly after crack initiation, with first a gradual and then a steep slope, different values of δ_t^c cause a sensible difference between the load–deflection curves. Figure 8(b) shows the normalized crack depth, a/t vs loading-point displacement, $\delta^{\mathrm{tot}}/l_0$ under pure extension. The crack in the longer specimen grows faster than that in the shorter specimen, and delayed initiation of crack growth simply shifts the curve to the right, as illustrated by dashed lines. Figure 8(c) compares the line-spring solution with the continuum FEM solution based on the nodal release technique and the same CTOA criterion (Jung, 1995), for nonhardening material. To capture the intensive global deformations on $\pm 45^{\circ}$ slip-lines emanating from the moving crack-tip in pure extension, the continuum FEM approach used about 3500 plane strain 4-node elements. To the extent ($\delta^{\mathrm{tot}}/l_0 \approx 0.13$) where continuum FEM solution was obtained, both solutions agree very well. While the line-spring solution required only

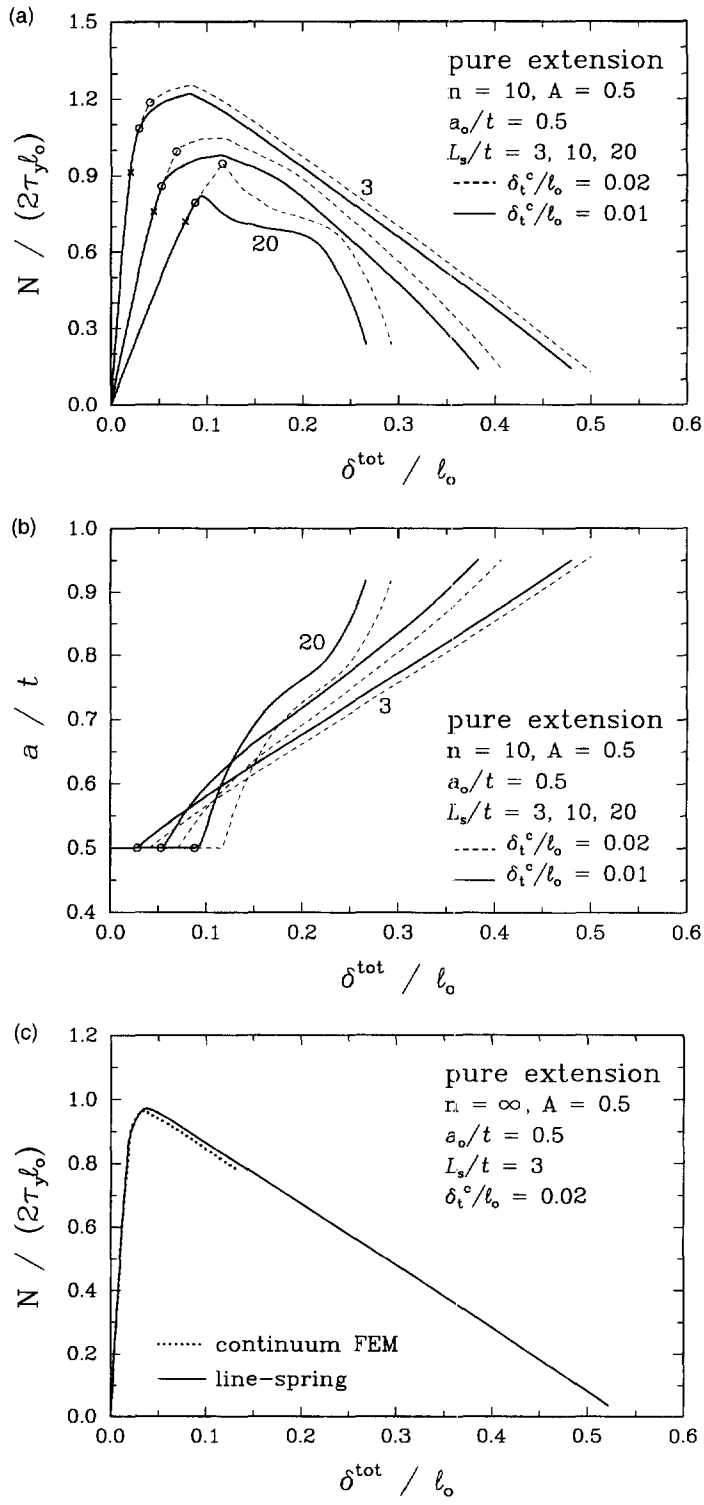

Fig. 8. (a) Normalized axial force $N/(2\tau_y l_0)$ vs loading-point total displacement δ^{tot}/l_0 of the plane strain SEC specimen with initial relative crack depth $a_0/t = 0.5$ under pure extension ($N > 0$, $\theta^{\infty} = 0$). Solid lines are based on the critical CTOD value $\delta_t^c/l_0 = 0.01$, and dashed lines based on $\delta_t^c/l_0 = 0.02$. (b) Normalized crack a/t vs loading-point total displacement δ^{tot}/l_0 under pure extension. (c) Comparison between line-spring solution and continuum finite element solution based on nodal release technique (Jung, 1995).

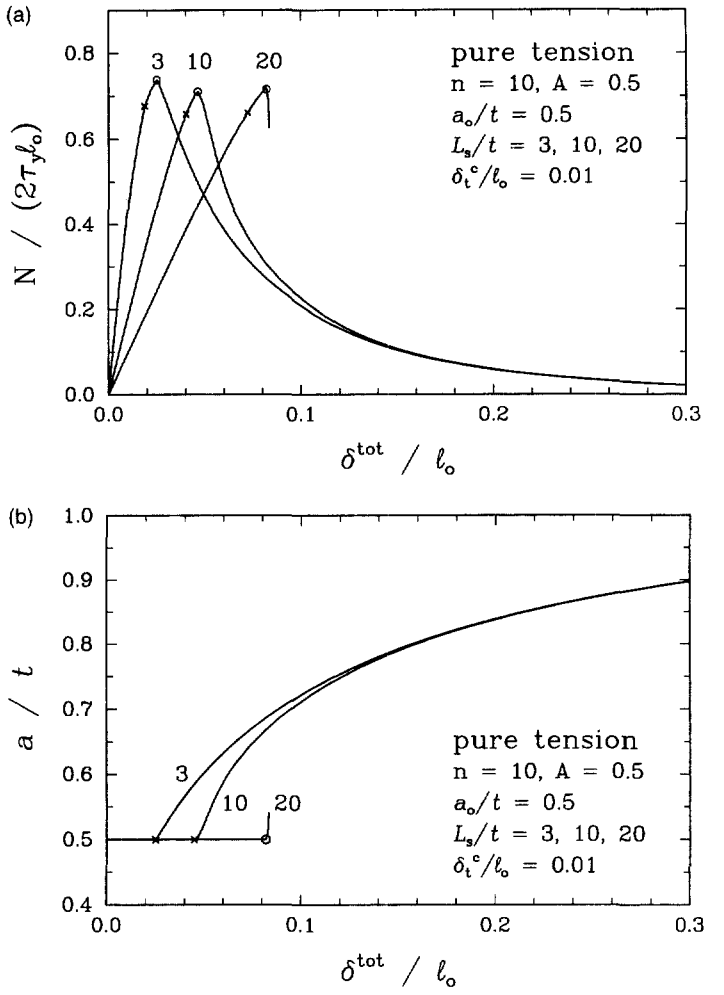

Fig. 9. (a) Normalized axial force vs loading-point total displacement of the plane strain SEC specimen with initial relative crack depth $a_0/t = 0.5$ under remote pure tension ($N > 0$, $M = 0$). (b) Relative crack depth a/t vs loading-point total displacement δ^{tot}/l_0 under remote pure tension for various relative specimen lengths.

a few minutes on an HP 9000 workstation, the continuum FEM solution took two orders of magnitude longer on the same workstation.

Figure 9(a) presents the normalized axial force vs load-point displacement of the plane strain SEC specimen with initial relative crack depth $a_0/t = 0.5$ under remote pure tension ($N > 0$, $M = 0$). Again, the cross symbol indicates the initial fully plastic yielding, and the open circle indicates the commencement of crack growth. In pure tension, even in short and intermediate specimens ($L_s/t = 3$, 10), loading decreases immediately after crack initiation, in contrast to pure extension. In the specimen of $L_s/t = 20$, the load–deflection curve drops almost vertically, which can be viewed as a kind of instability in the static crack extension. Figure 9(b) reveals that the crack in the long specimen is initially delayed, then growth per unit loading-point displacement ($\Delta a/\Delta\delta^{tot}$) becomes larger than that in the short specimen under pure tension. The vertical load drop and the abrupt crack extension depicted by the dashed lines based on $\delta_t^c/t = 0.02$ in Fig. 10(a) and (b) illustrate that the retardation of crack initiation in a long specimen ($L_s/t = 15$) can induce the crack to behave unstably. When the plane strain SEC specimen is loaded in a pure bending mode as shown in Fig. 11(a) and (b), the crack tends to grow more stably.

In Fig. 12(a), normalized axial force vs total loading-point displacement curves of plane strain SEC specimen having $a_0/t = 0.5$, and $L_s/t = 20$ under remote pure tension are plotted for $\delta_t^c/l_0 = 0.01$, respectively, and differing material values of A, with $B(\sigma_s) = 0$.

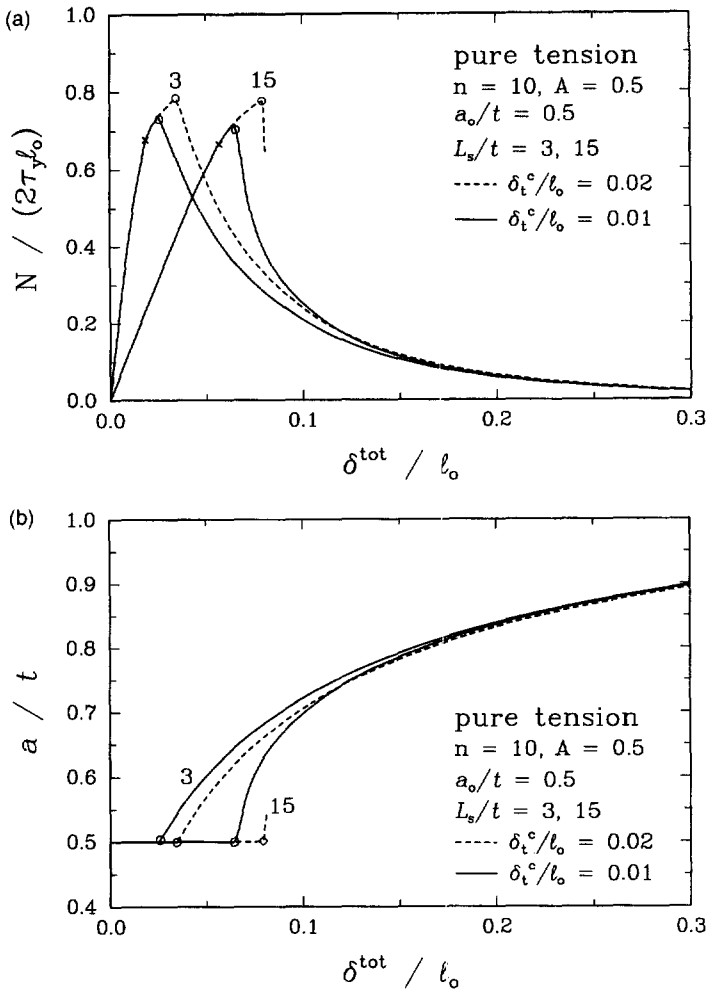

Fig. 10. (a) Effect of critical CTOD value for initiation on the load-deflection curve of SEC specimen with initial relative crack depth $a_0/t = 0.5$ under remote pure tension. (b) Crack extensions in the SEC specimen for two different values $\delta_t^c/l_0 = 0.01$, 0.02 and for two different relative specimen half-lengths $L_s/t = 3$, 15.

The values $A = 1.175$ and $B = 0$ correspond to a hole growth ratio $R_f/R_0 = 1.8$ and fracture strain $\gamma_f = 1$ for $\sigma_s/(2\tau_0) = 0.5$. When carefully compared with Fig. 9(a), Figure 12(a) demonstrates that the crack in the same specimen, but composed of more ductile material with $A = 1.175$, can be made to grow stably. In Fig. 12(b), effects of tensile yield strength relative to elastic modulus (σ_y/E) on the stability of plane strain SEC specimens of non-hardening materials under pure tension are examined, again for $\delta_t^c/l_0 = 0.01$. Cracking in higher strength material shows more propensity for instability. For material ductilities $A = 0.5$ and 0.8, the response of plane strain SEC specimens having $L_s/t = 20$ and three different initial relative crack depths ($a_0/t = 0.4$, 0.5 and 0.6) subjected to remote pure tension are given in Fig. 13(a) and (b). In the specimen of $a_0/t = 0.6$, the crack grows stably for both materials, whereas in the $a_0/t = 0.5$ case, initial cracking is unstable for $A = 0.5$, but stable for $A = 0.8$. Cracks in the specimen of $a_0/t = 0.4$ grow unstably for both material ductilities considered. In brief, the higher fully plastic loads of initially shorter cracks tend to incline the system to unstable cracking.

Effects of material hardening are examined in Fig. 14(a) and (b) for pure extension and pure bending, respectively. Under pure extension, the reaction force in hardening material ($n = 10$) first increases then decreases, while that in nonhardening material ($n = \infty$) decreases almost immediately following crack initiation. The reaction moments in pure bending, however, decrease after crack initiation regardless of material hardening, at least

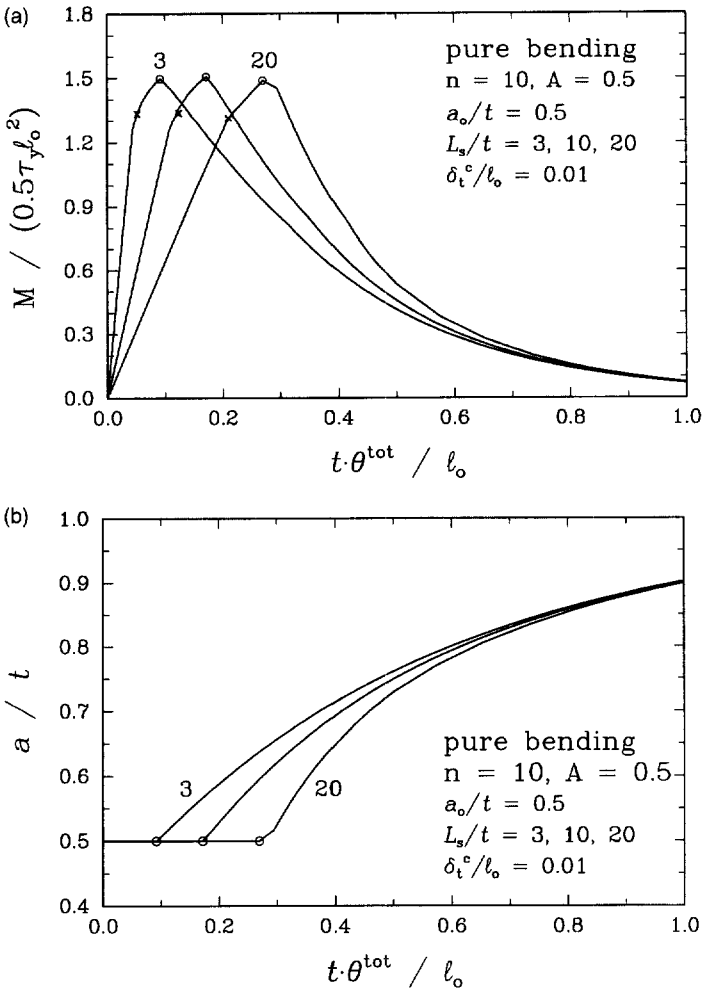

Fig. 11. (a) Normalized bending moment vs loading-point rotation of a deeply cracked SEC specimen under pure bending mode. (b) Stable crack extensions in a deeply cracked specimen regardless of relative specimen lengths, when subject to pure bending.

for the tested cases ($n = \infty$ and $n = 10$). The reaction moment in pure bending is proportional to the square of the ligament length, while the reaction force in pure extension is proportional to the ligament length itself. It thus seems that in pure bending, the load reduction due to net ligament decrease more than offsets any load increase due to strain hardening. The reaction force and moment of SEC specimens with initial relative crack depths $a_0/t = 0.4$ and 0.6 under pure extension ($N > 0$, $\theta^{\infty} = 0$) are plotted against the relative crack depth a/t in Fig. 15(a) and (b). Once the response of the initially short crack ($a_0/t = 0.4$) gets on the track of the initially deep crack ($a_0/t = 0.6$), no effect of initial crack depth is observed. However, the loci of reaction forces merge at $a/t \approx 0.64$, while the loci of reaction moments merge at $a/t \approx 0.68$, a bit later.

As another type of "2-D" problem, we study externally part-through, complete circumferential cracks in pipes under remote uniaxial tension. Figure 16(a) shows that in nonhardening material, the axial forces fall immediately after crack initiation, which points are marked by open circles. Axial force F is normalize with the mean shell radius R_m, the initial yield strength in shear τ_y, and initial ligament length l_0. For the shell of relative radius $R_m/t = 400$, the load vs displacement curve recovers the shape of the plane strain SEC specimen case of Fig. 8(a). On the other hand, as shown in Fig. 16(b), the reaction force of hardening material continues to increase even after crack initiation, and reaches a maximum for the shells of $R_m/t = 10$, 100, 200. For $R_m/t = 400$, the hardening curve is similar to the nonhardening case except for the higher maximum load. It is also observed

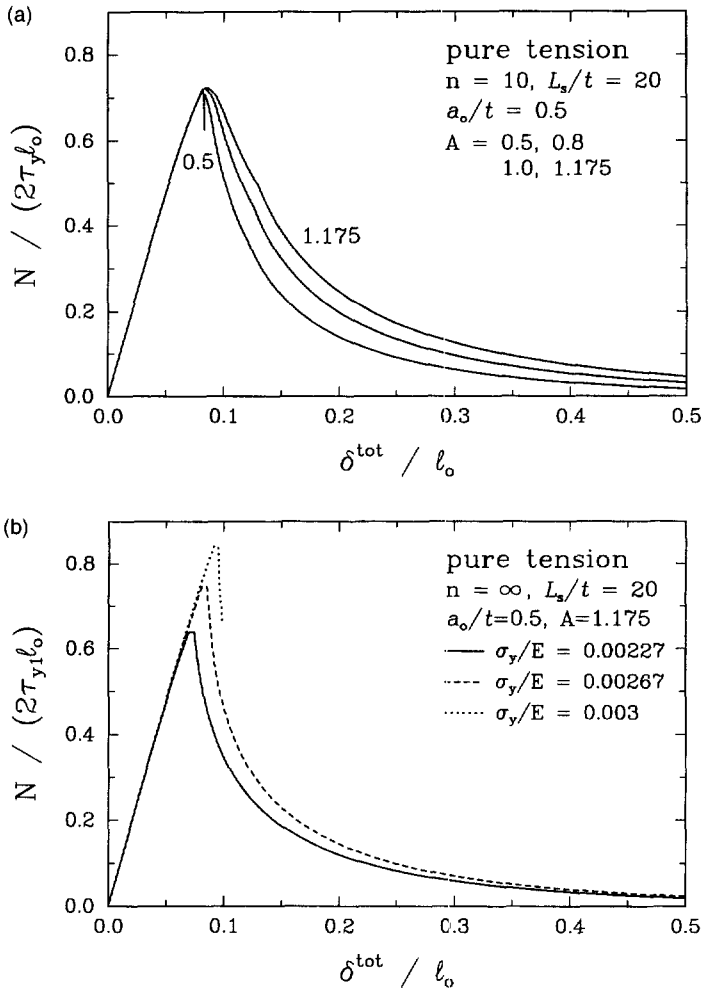

Fig. 12. (a) Normalized axial force vs total loading-point displacement curves of plane strain SEC specimen having $a_0/t = 0.5$, and $L_s/t = 20$ under remote pure tension for various material values of A with $B(\sigma_s) = 0$. (b) Effects of yield strength on the stability of plane strain SEC specimens of nonhardening materials under remote pure tension are demonstrated. Higher strength material shows more propensity for instability.

that the shell of smaller R_m initiates later in hardening material. Figure 16(c) illustrates that increasing material ductility retards the load leveling-off, thus stabilizing the system. The negligible influence of shell length on the shape of load–deflection curve in Fig. 16(d) contrasts with the plane strain case ($R_m \to \infty$) of Fig. 8(a). Thus, the curvature of the shell ($R_m/t = 10$) tends to stabilize the system of $L_s/t = 20$ specimen.

5. DISCUSSION

In the results in Fig. 8(a) to Fig. 13(a), nonlinearity due to contained yielding was in fact captured using a modified effective crack length (Hauf *et al.*, 1995; Lee and Parks, 1995). However, as manifested by the load–deflection curves preceding the " × " symbols, nonlinearity in $\Phi < 0$ is barely perceptible in the displacement scale of our current interest, which involves fully plastic crack initiation and extension over a sizable portion of the initial ligament. Therefore, for purposes of simplification, in Section 3 we left out the effective crack length formulation (Lee and Parks, 1995), and describe the deformation in $\Phi < 0$ to be purely elastic; however, including initial nonlinearity due to contained yielding is straightforward.

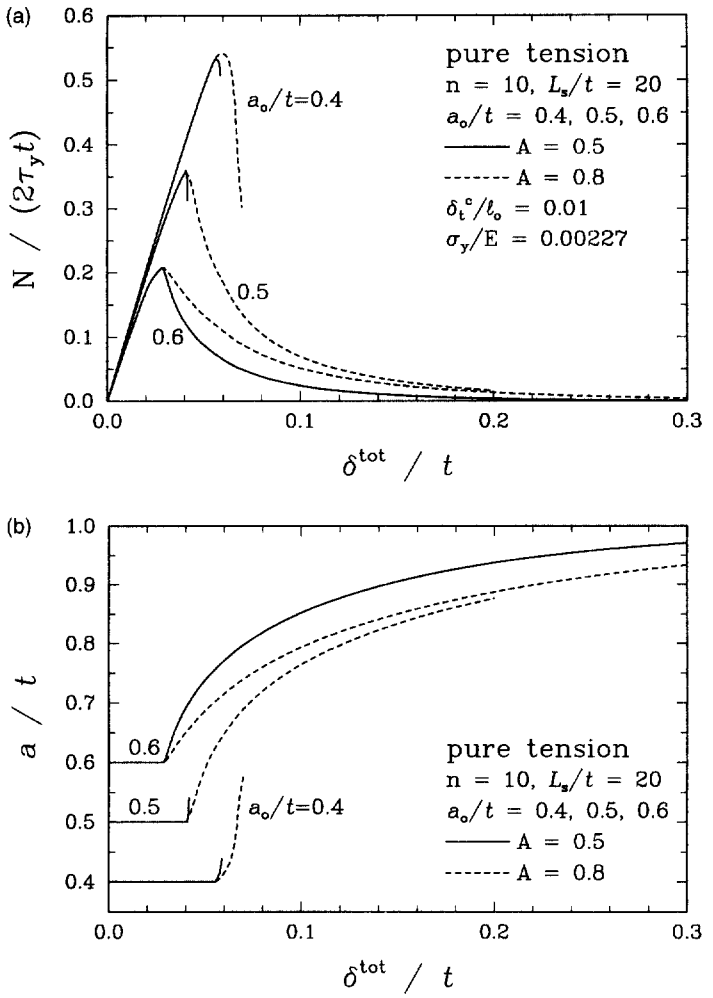

Fig. 13. (a) The responses of plane strain SEC specimens having $L_s/t = 20$ and three different initial relative crack depths $a_0/t = 0.4$, 0.5 and 0.6 subjected to remote pure tension. (b) Crack extension stability dependence on the initial relative crack depth a_0/t, and material ductility A.

Instability for a plane strain SEC specimen loaded by remote pure tension under overall displacement control can be analyze as follows. First, the increment of total load-point displacement is given by

$$d\delta^{\text{tot}} = \mathrm{d}\delta^{(e,c)} + \mathrm{d}\delta^{(e,nc)} + \mathrm{d}\delta^{(p,c)} + \mathrm{d}\delta^{(p,nc)}$$
$$= \left[\frac{2}{E'}\int_0^a F_1^2(\bar{a}, t)\,\mathrm{d}\bar{a} + \frac{2Ls}{E't}\right]\mathrm{d}N + \mathrm{d}\delta^{(p,c)} + 0. \tag{19}$$

Here superscript "(e, c)" denotes the elastic part of the load-point displacement due to the crack, and "(e, nc)" denotes that part absent the crack. The superscript "p" denotes the corresponding plastic part of displacement. Using (13) relating $\mathrm{d}\delta^{(p,c)}$ to $\mathrm{d}\delta_t^{(p)}$ and (12) connecting $\mathrm{d}\delta_t^{(p)}$ to $\mathrm{d}a$, the last term on the right side of (19) can be expressed as

$$\mathrm{d}\delta^{(p,c)} = 2\tan\left(\frac{\mathrm{CTOA}}{2}\right)\cdot\left[1 + L_2\cdot\left(\frac{1}{2} - \frac{a}{t}\right)\cdot\left(\frac{t\Delta\theta^{(p)}}{\Delta\delta^{(p)}}\right)\right]^{-1}\mathrm{d}a$$
$$\equiv 2\tan\left(\frac{\mathrm{CTOA}}{2}\right)\cdot[1 + D]^{-1}\,\mathrm{d}a. \tag{20}$$

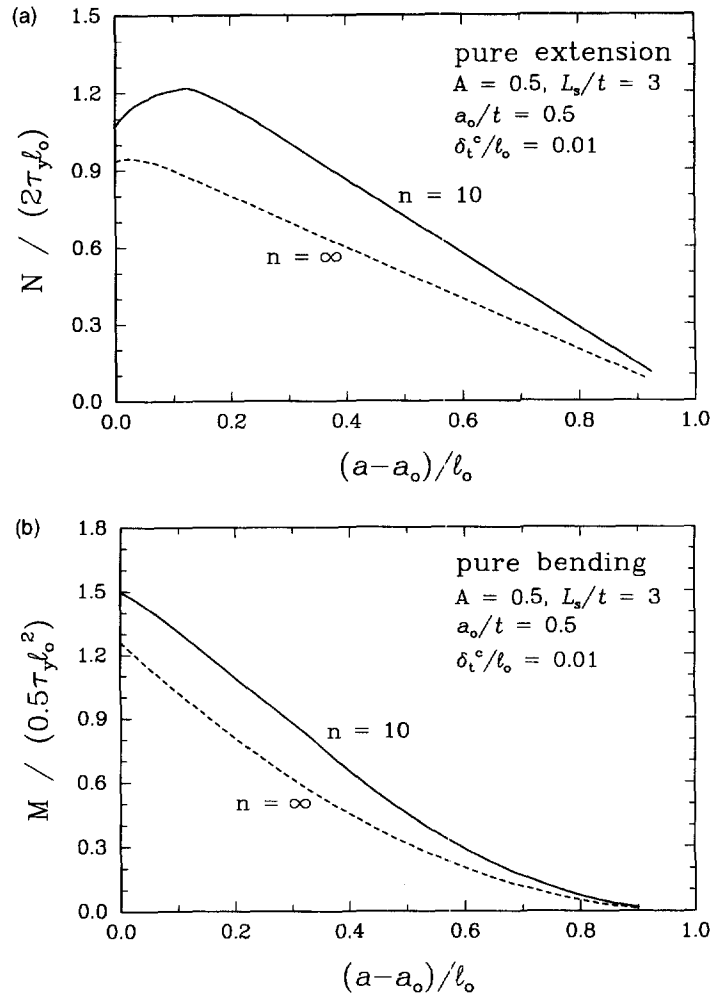

Fig. 14. (a) Effect of material hardening on the reaction force against crack extension curve for pure extension. (b) Effect of material hardening on the reaction moment against crack extension curve for pure ending.

When a nonhardening deeply-cracked SEC specimen undergoing cracking remains at yield under remote pure tension, the load is $N = C_1 \cdot 2\tau_0 l$, where $C_1 = \hat{C}_1(a/t)$ can be determined from the appropriate branch of the yield surface, from (6) or (7), with $M = 0$. Substituting $dN = d(C_1 \cdot 2\tau_0 l)$ into (19) along with (20), provides

$$\frac{da}{d\delta^{tot}} = \left\{\frac{2\tan(CTOA/2)}{1+D} - \frac{4\tau_0 C_2}{E'}\left[\int_0^a F_1^2(\bar{a}, t)\, d\bar{a} + \frac{L_s}{t}\right]\right\}^{-1} \tag{21}$$

where $C_2 = C_1 - l\partial C_1/\partial a$. Under displacement-controlled loading, the crack growth becomes unbounded when the quantity inside the braces on the right side of (21) vanishes.

The stability condition expressed by (21), as well as broad conclusions which can be deduced from it, is reminiscent of J-based tearing stability models developed by Paris and co-workers (1979), but with several important differences. First, the roles of increasing strength (τ_0/E) and specimen length (L_s/t) in destabilizing cracking are evident in (21), as is the stabilizing role of increasing ductility through CTOA. The strength effect may be either intrinsic (τ_y) or elevated by prior strain hardening in the ligament (τ_0). The role of relative crack depth a/t in affecting stability is more complex, since it directly influences C_2 and D through the size (C_1) and shape of the yield surface at remote tension. When $M = 0$, $\mu = a/l$ and the MGH yield surface (7) is applicable for $a/2l \geq 0.6$, or $a/t \geq 0.55$. In this

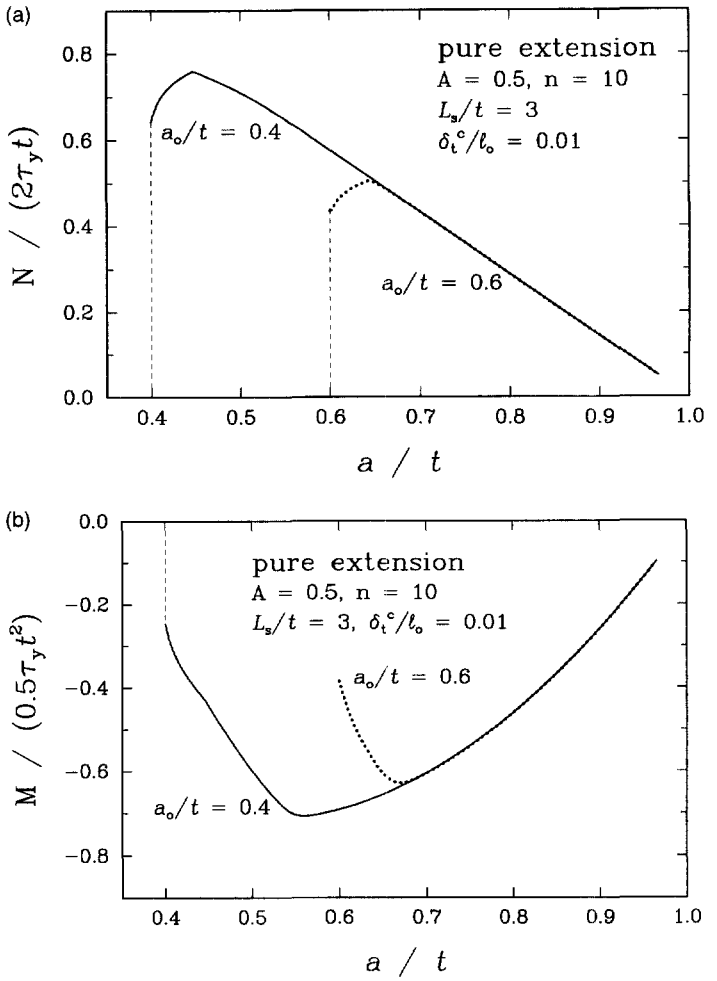

Fig. 15. (a) Reaction force vs relative crack depth a/t of SEC specimens with $a_0/t = 0.4$ and 0.6 under pure extension. (b) Reaction moment vs relative crack depth a/t of SEC specimens with $a_0/t = 0.4$ and 0.6 under pure extension.

regime, $L_2 = 1$ and the negative term D monotonically decreases with a/t to -1 at $a/t \to 1$, while C_2 monotonically decreases to zero as $a/t \to 1$. Thus, as $a/t \to 1$ and the ligament comes to be loaded in predominant bending, there is (ultimately) strong tendency for stable cracking in tension, as seen in Figs 9, 10, 12 and 13, notwithstanding the possibility of early instability. The terminal stability of the bending solutions in Figs 11 and 14(b) is similarly consistent with (21), although a separate analysis of (pure) bending analogous to that leading to (21) would be more revealing. A further complexity of the present model lies in the possible variability of CTOA. For example, in remote pure tension, if initial crack depth lies in $\sim 0.35 \leqslant a_0/t \leqslant 0.55$, then increasing crack length in this interval results in a progressively decreasing CTOA.

For the limiting case of rigid-plastic, nonhardening materials, Kim (1993) presented a plane strain, fully plastic crack growth line-spring model. With large-geometry change of elastic surroundings included, their model effectively accounts for the bulging response of a cracked part. Bulging causes the line of action of applied load to shift relative to the plate centerline and produces less bending moment on the ligament. The effect of bulging is more pronounced for tension of long specimens under pinned boundary conditions, where remote applied mid-specimen moment is zero. Our line-spring model formulated on small geometry change does not describe such bulging behavior. However, unlike the through-crack in a 2-D SEC specimen, finite length surface cracks embedded in plates/shells experience more severe geometrical resistance to bulging from their elastic surroundings. Accordingly, the

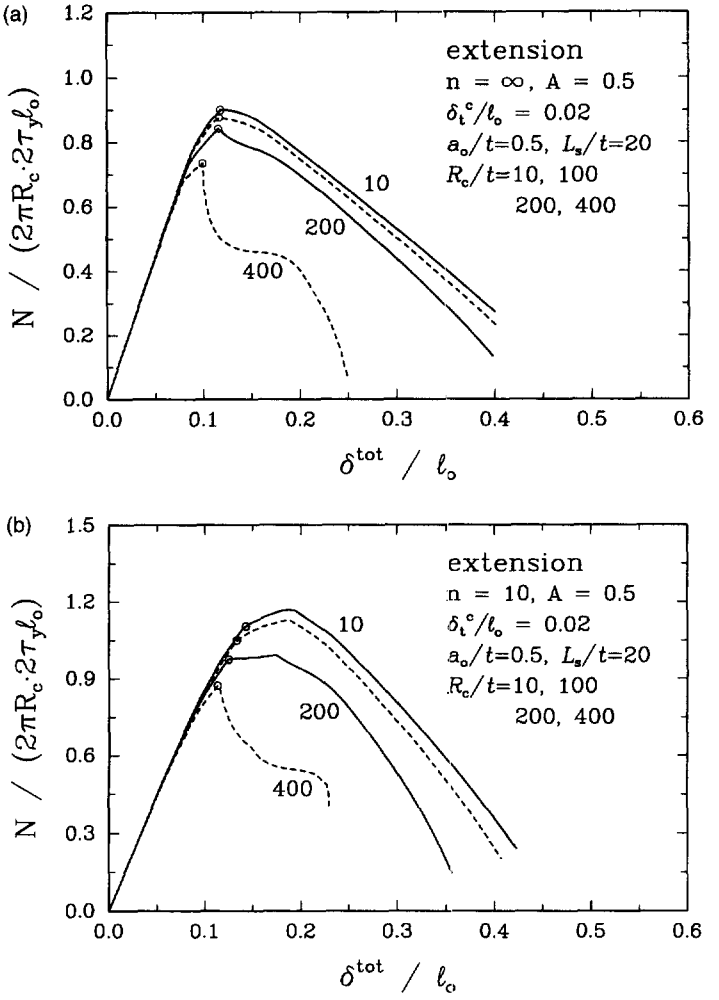

Fig. 16. Normalized axial force $F/(2\pi R_m \cdot 2\tau_y l_0)$ vs loading-point total displacement δ^{tot}/l_0 of axisymmetrically cracked pipes under uniaxial tension for various R_m/t ratios. (a) $n = \infty$. (b) $n = 10$. (c) Effect of material ductility on normalized axial force vs loading-point total displacement curve of axisymmetrically cracked pipes under uniaxial tension. (d) Effect of shell curvature on the system stabilization. In contrast to the plane strain case ($R_m \to \infty$) of Fig. 8(a), there is no influence of shell length on the shape of load–deflection curve.

bulging effect is expected to be less important in surface crack problems presented in Part II (Lee and Parks, 1998). In any event, since bulging plays the beneficial role of relieving the crack-tip constraint (μ decreases, hence CTOA increases), a crack growth simulation based on small-geometry change analyses can be regarded as conservative.

When a crack advances through elastic/perfectly–plastic material under plane strain mode I small-scale yielding, the crack-tip strain singularity is weaker than that of the stationary crack (Rice, 1975). The strain field at the growing crack-tip is not thoroughly refocused because of crack extension into the plastically deformed material. This reduced crack-tip strain concentration is the main source of stable crack growth. Our present fully plastic analyses of crack growth assume that the deformation fields of growing cracks are incrementally identical to those of a stationary crack. This assumption seems to overestimate the strain singularity at the fully plastic growing crack-tip, when judged qualitatively by comparing strain singularities at the tips of stationary and growing cracks under SSY condition.

Our line-spring treatment of fully plastic hardening of material during ductile crack growth, though plausible, merits further study. As the crack-tip advances, the hardened material convects out from, and fresh material enters into, the active plastic region. Since

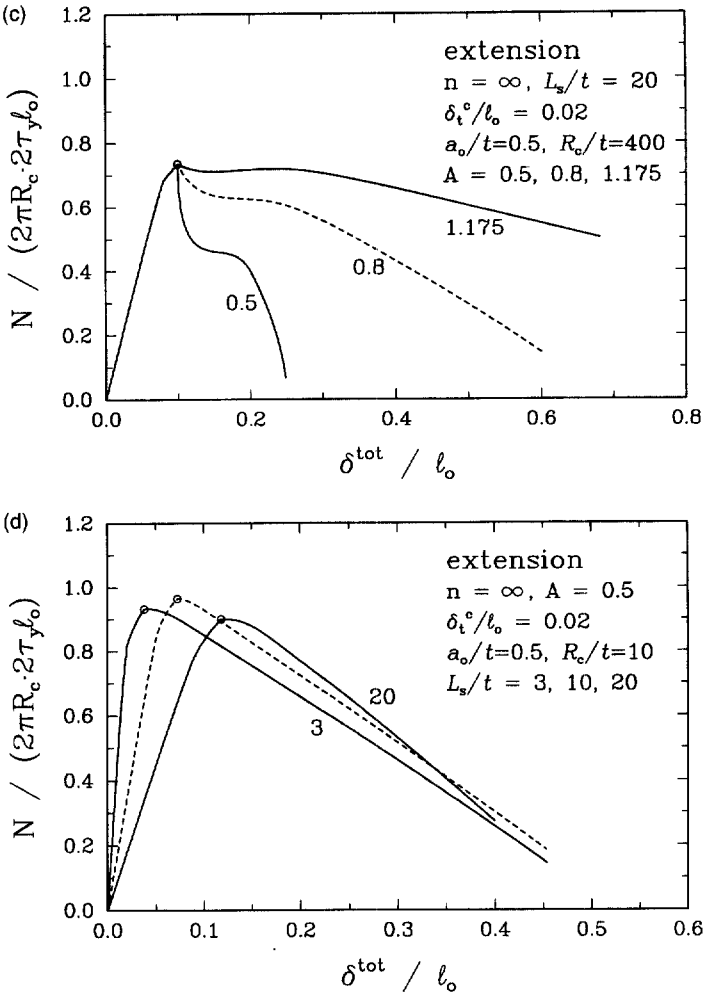

Fig. 16.—*Continued.*

our current line-spring model does not directly account for this convection out of hardened material, we expect that the model overestimates the ligament-average hardness in the active plastic region. Moreover, hardening is spatially nonuniform in the ligament, with highest flow strength near the tip. In the continuum, for example, this forces higher bending moments and triaxiality under pure extension (Jung, 1995).

6. SUMMARY

In this study, we presented a line-spring model which can simulate the crack growth of plane strain SEC specimens as well as surface cracks in plate/shell structures under fully plastic plane strain condition. CTOA is treated as a material-dependent function of the stress and deformation imposed on the growing crack-tip region. We approximately evaluated the CTOA in terms of loads within line-spring finite elements, by integrating the sliding-off and cracking model of McClintock *et al.* (1995), and the least upper bound method of Kim *et al.* (1996a). Upon determining the constraint-dependent CTOA and the loading-imposed increment of CTOD, we kinematically calculate the increment of crack extension.

Parametric studies were performed on 2-D plane strain SEC specimens. The increase of generalized force after crack initiation depends on the loading type and material hardening. The increase of reaction force of a short SEC specimen under pure extension comes from the strain hardening, and the drift of load state towards the vertex of the yield surface. The crack in the longer specimen grows faster (per unit imposed deformation) than that in

the shorter specimen for pure extension, while a reversal occurs for remote pure tension. Hardening material naturally provides a larger maximum reaction force/moment than nonhardening material. Retardation of crack initiation, longer specimen length, higher yield strength, lower ductility and an initially shorter crack, each tends to make the crack of SEC specimens grow more unstably. In a tensile-loaded pipe with a complete circumferential crack, the curvature of the shell tends to stabilize the system. Stability of fully plastic plane strain cracking of SEC specimen under remote pure tension was discussed in terms of line-spring system characteristics.

Acknowledgments—This work was supported by the Office of Basic Energy Sciences, Department of Energy, under Grant No. DE-FG02--85ER13331. Computations were performed on Sun Sparc workstations obtained under ONR Grant No. 0014-89-J-3040, and HP 9000 workstations obtained under NSF grant No. DDM-8914161. The ABAQUS finite element program was made available under academic license from Hibbit, Karlsson and Sorensen, Inc., Pawtucket, RI. We would like to thank Professor F. A. McClintock of MIT and Dr. Y.-J. Kim of GKSS for many helpful discussions.

REFERENCES

ABAQUS User's Manual (1993) Version 5.3, Hibbitt, Karlsson and Sorensen, Inc., Pawtuket, RI.

Amazigo, J. C. and Hutchinson, J. W. (1977) Crack-tip fields in steady crack-growth with linear strain-hardening. *Journal of the Mechanics and Physics of Solids*. **25,** 81–97.

Drugan, W. J. and Chen, X. Y. (1989) Plane strain elastic–ideally plastic crack fields for mode I quasistatic growth at large-scale yielding—I. A new family of analytical solutions. *Journal of the Mechanics and Physics of Solid* **37,** 1–26.

Drugan, W. J., Rice, J. R. and Sham, T.-L. (1982) Asymptotic analysis of growing plane strain tensile cracks in elastic–ideally plastic solids. *Journal of the Mechanics and Physics of Solids* **30,** 447–473.

Ewing, D. J. F. (1968) Calculation on the bending of rigid/plastic notched bars. *Journal of the Mechanics and Physics of Solids* **16,** 205–213.

Gibson, G. P. and Druce, S. G. (1987) An assessment of various crack tip displacement based elastic–plastic fracture parameters to characterise ductile crack growth resistance. *International Journal of Fracture* **35,** 139–151.

Green, A. P. (1956) The plastic yielding of shallow notched bars due to bending. *Journal of the Mechanics and Physics of Solids* **4,** 259–268.

Green, A. P. and Hundy, B. B. (1956) Initial plastic yielding in notch bend tests. *Journal of the Mechanics and Physics of Solids* **4,** 128–144.

Gudmundson, P. (1989) Validity of asymptotic crack tip solutions for plastic materials. In *Advances in Fracture Research*, Vol. 1, Proceedings of the 7th International Conference on Fracture, ed. K. Salama *et al.*, pp. 315–322. Houston, U.S.A., Pergamon, Oxford.

Hancock, J. W., Reuter, W. G. and Parks, D. M. (1993) Constraint and toughness parameterized by T. In *Constraint Effects in Fracture*, ASTM STP 1171, ed. E. M. Hackett *et al.*, pp. 21–40.

Hauf, D. E., Parks, D. M. and Lee, H. (1995) A modified effective crack-length formulation in elastic–plastic fracture mechanics. *Mechanics of Materials* **20,** 273–289.

Hutchinson, J. W. and Paris, P. C. (1979) Stability analysis of J-controlled crack growth. In *Elastic–Plastic Fracture*, ASTM STP 668, ed. J. D. Landes *et al.*, pp. 37–64.

Jung, S. H. (1995) Growing crack analyses using nodal release technique. M.S. thesis, Department of Mechanical Engineering, Massachusetts Institute of Technology, Cambridge, MA.

Kardomateas, G. A. and McClintock, F. A. (1989) Shear band characterization of mixed mode I and II fully plastic fracture. *International Journal of Fracture* **35,** 1–12.

Kim, Y.-J. (1993) Modeling fully plastic, plane strain crack growth. Ph.D. dissertation, Department of Mechanical Engineering, Massachusetts Institute of Technology, Cambridge, MA.

Kim, Y.-J., McClintock, F. A. and Parks, D. M. (1996a) Global equilibrium of the least upper bound circular arcs and its application to fracture mechanics. *International Journal of Fracture*, accepted.

Kim, Y.-J., McClintock, F. A. and Parks, D. M. (1996b) Yield locus in deep, single-face cracked specimens under combined bending and tension. *Journal of Applied Mechanics* **63,** 1045–1047.

Lee, H. and Parks, D. M. (1993) Fully plastic analyses of plane strain single-edge cracked specimens subject to combined tension and bending. *International Journal of Fracture* **63,** 329–349.

Lee, H. and Parks, D. M. (1995) Enhanced elastic–plastic line-spring finite element. *International Journal of Solids and Structures* **32,** 2393–2418.

Lee, H. and Parks, D. M. (1998) Line-spring finite element for fully plastic crack growth—II. Surface cracked plates and pipes. *International Journal of Solids and Structures* **35,** 5139–5158.

McClintock, F. A., Kaplan, S. M. and Berg, C. A. (1969) Ductile fracture by hole growth in shear bands. *International Journal of Fracture Mechanics* **17,** 201–217.

McClintock, F. A. (1969) Crack growth in fully plastic grooved tensile specimens. In *Physics of Strength and Plasticity*, Orowan Anniversary Volume, ed. A. S. Argon, pp. 307–326. MIT Press, Cambridge.

McClintock, F. A. and Wineman, S. J. (1987) A wedge test for quantifying fully plastic fracture. *International Journal of Fracture* **33,** 285–295.

McClintock, F. A., Kim, Y.-J. and Parks, D. M. (1995) Tests for fully plastic fracture mechanics of plane strain mode I crack growth. In *Constraint Effects in Fracture: Theory and Applications*, ASTM STP 1256, ed. M. Kirk and A. Bakker, pp. 199–222.

Miyoshi, T., Shiratori, M. and Yoshida, Y. (1986) Analysis of J-integral and crack growth for surface cracks by line-spring method. *Journal of Pressure Vessel Technology* **108,** 305–311.

Paris, P. C., Tada, H., Zahoor, A. and Ernst, H. (1979) The theory of instability of the tearing mode of elastic–plastic crack growth. In *Elastic–Plastic Fracture*, ASTM STP 668, ed. J. D. Landes *et al.*, pp. 5–36.

Parks, D. M. (1981) The inelastic line-spring: estimates of elastic–plastic fracture mechanics parameters for surface-cracked plates and shells. *J. Press. Vessel Tech.* **103,** 246–254.

Parks, D. M. and White, C. S. (1982) Elastic–plastic line-spring finite elements for surface-cracked plates and shells. *Journal of Pressure Vessel Technology* **104,** 287–292.

Ponte Castañeda, P. (1987) Asymptotic fields in steady crack growth with linear strain-hardening. *Journal of the Mechanics and Physics of Solids* **35,** 227–268.

Reuter, W. G. and Lloyd, W. R. (1990) Measurements of CTOD and CTOA around surface-crack perimeters and relationships between elastic and elastic–plastic CTOD values. In *Surface-Crack Growth: Models, Experiments, and Structures*, ASTM STP 1060, ed. W. G. Reuter *et al.*, pp. 152–176.

Rice, J. R. (1972a) The line-spring model for surface flaws. In *The Surface Crack: Physical Problems and Computational Solutions*, ed. J. L. Swedlow, pp. 171–185. American Society of Mechanical Engineers, New York.

Rice, J. R. (1972b) Some remarks on elastic crack tip fields. *International Journal of Solids and Structures* **8,** 751–758.

Rice, J. R. (1975) Elastic–plastic models for stable crack growth. In *Mechanics and Mechanisms of Crack Growth*, Proceedings of Conference at Cambridge, U.K., ed. M. J. May, pp. 14–39. British Steel Corporation Physical Metallurgy Center Publication.

Rice, J. R. and Levy, N. (1972) The part-through surface crack in an elastic plate. *Journal of Applied Mechanics* **39,** 185–194.

Rice, J. R. and Sorensen, E. P. (1978) Continuing crack-tip deformation and fracture for plane-strain crack growth in elastic–plastic solids. *Journal of the Mechanics and Physics of Solids* **26,** 163–186.

Tada, H., Paris, P. C. and Irwin, G. R. (1985) *The Stress of Cracks Handbook*. Fracture Proof Design, Saint Louis, MO.

Wang, Y.-Y. (1993) On the two-parameter characterization of elastic–plastic crack-front fields in surface-cracked plates. In *Constraint Effects in Fracture*, ASTM STP 1171, ed. E. M. Hackett, K.-H. Schwalbe and R. H. Dodds Jr., pp. 120–138.

Wang, Y.-Y. and Parks, D. M. (1992) Evaluation of the elastic T-stress in surface-cracked plates using the line-spring method. *International Journal of Fracture* **56,** 25–40.

White, C. S., Ritchie, R. O. and Parks, D. M. (1983) Ductile growth of part-through surface cracks: experiment and analysis. In *Elastic–Plastic Fracture: Second Symposium, Volume I—Inelastic Crack Analysis*, ASTM STP 803, ed. C. F. Shih and J. P. Gudas, pp. I-384–I-409.